HiSST: International Conference on
High-Speed Vehicle Science Technology

26–29 November 2018, Moscow, Russia

A Simple Extending Strategy for TENO Scheme: scalar equation and Euler equations

Fan Zhang[1], Chunguang Xu[2], Jun Liu[3]

Abstract

A simple extending strategy is presented to improve the efficiency and accuracy of the state-of-the-art high order TENO schemes [1]. The presented method applies the smooth measurement of TENO to detect the position of discontinuity and then uses a polynomial selection procedure to directly apply spatial reconstruction of high-order accuracy, without crossing any discontinuity. Especially, neighbouring grid points contained in smooth stencils is also applied in spatial reconstruction to increase the order of polynomials, and thus the accuracy is improved with little extra computational cost. Since the reconstruction crossing discontinuity is completely avoided, ENO-property is attained. Numerical simulations including scalar equation and Euler equations are presented to testify the performance of the new method. The presented method gives results of which the accuracy is of seventh-order in smooth field, and the complexity of the method is similar to that of the fifth-order TENO.

Keywords: TENO, extending strategy, polynomial selection, ENO-property

1. Introduction

The spatial solutions of flow field containing discontinuities are extremely challenging, because of the nonlinear essential of the governing equations. Especially, achieving high-order accuracy on smooth flow field including critical points and eliminating oscillation near discontinuities are two crucial issues that are attracting attentions, due to their necessities as well as their difficulties. Without stressing the details here, we only need to recall the fact that high-order interpolation will produce spurious oscillation near discontinuities, leading to troublesome problems such as positivity issues and erroneous solutions.

In order to solve those problems, various methodologies have been developed. Recently, Targeted ENO (TENO) schemes have been invented by Fu et al. [1]. Instead of reducing the contribution of oscillatory stencils by the nonlinear weighting strategy of WENO schemes, TENO schemes completely remove the oscillatory stencils in the final reconstruction, and fully recover the background linear scheme if all the candidate stencils are deemed to be smooth. So far, various numerical results including turbulence flows [12], multi-phase flows [13] and detonations [14], have proved that TENO schemes are accurate and robust. Most importantly, TENO schemes, in fact, give a new way to fully discard the weighting procedure [15], facilitating the utilization of the candidate stencils and the development of higher-order schemes.

Usually, in order to increase the order of accuracy of a specific numerical scheme, more degree-of-freedoms (DOFs) are necessary for constructing higher-order polynomials. For finite difference schemes such as WENO or TENO, more DOFs are usually given by extending the candidate stencil(s). For example, instead of using three three-point stencils in a five-point WENO scheme, the seven-point WENO scheme uses four four-point stencils [16]. At the meantime, more complicate smoothness indicators are required for measuring oscillation and calculating the nonlinear weights, leading to higher computational cost. Since TENO schemes are developed to function as a discontinuity-location detector [15] and the

[1]School of Aeronautics and Astronautics, Sun Yat-sen University, zhangfan.zf@mail.ru
[2]School of Aeronautics and Astronautics, Sun Yat-sen University, springguang@msn.com
[3]State Key Laboratory of Structural Analysis for Industrial Equipment, Dalian University of Technology

high-order polynomial can be calculated separately, simpler smoothness indicators could be used for implementing higher-order spatial approximation, reducing computational cost.

Therefore, an extending strategy based on the TENO framework is given in this work. The following sections are organized as follows. In the next section, WENO and TENO schemes are briefly introduced, and especially the ENO-like stencil-selection procedure is specifically introduced for introducing following discussions. In section 3, the recent development in [15] is briefly introduced. In section 4, the presented method is introduced in detail. In section 5, several typical numerical cases are used to examine the performance of the presented method. Finally, the concluding remarks are given in the last section.

2. Hyperbolic conservation law and TENO schemes

The one-dimensional hyperbolic conservation law is used to briefly introduce the basic idea of TENO schemes.

2.1. The fundamental of the finite-difference solution

The one-dimensional hyperbolic conservation law is written as

$$\frac{\partial u}{\partial t}+\frac{\partial f(u)}{\partial x}=0, \tag{1}$$

in which the characteristic velocity is $\frac{\partial f(u)}{\partial u}$ and assumed to be positive, without loss of generality. Here, the spatial discretization of Eq.(1) is given on an equally spaced one-dimensional mesh, leading to an ODE (ordinary differential equation) system, i.e.

$$\frac{du_i}{dt}=-\frac{\partial f}{\partial x}|_{x=x_i}, \quad i=1,\cdots,n. \tag{2}$$

The partial derivatives in x-direction are approximated by using the finite difference formula, i.e.

$$\frac{du_i}{dt}=-\frac{1}{\Delta x}(h_{i+1/2}-h_{i-1/2}). \tag{3}$$

The flux function $h_{i\pm1/2}$ at half points can be implicitly defined by

$$f(x)=\frac{1}{\Delta x}\int_{x-\Delta x/2}^{x+\Delta x/2}h(\xi)d\xi, \tag{4}$$

and the semi-discretized form can be written as

$$\frac{du_i}{dt}\approx-\frac{1}{\Delta x}(\hat{f}_{i+1/2}-\hat{f}_{i-1/2}), \tag{5}$$

where the numerical flux functions $\hat{f}_{i\pm1/2}$ are calculated from the convex combination of r candidate-stencil fluxes

$$\hat{f}_{i\pm1/2}=\sum_{k=0}^{r-1}\omega_k\hat{f}_{k,i\pm1/2}. \tag{6}$$

In order to obtain a $(2r-1)$-order approximation for flux functions $\hat{f}_{i\pm1/2}$, the $(r-1)$-order interpolation on each candidate stencil is given as

$$h(x)\approx\hat{f}_k(x)=\sum_{l=0}^{r-1}a_{l,k}x^l, \tag{7}$$

where the coefficients $a_{l,k}$ can be calculated by substituting Eq.(7) into Eq.(4) and solving the resulting linear algebraic system.

By applying the spatial approximation of the flux function, the temporal differential term in the ODE system, i.e. Eq.(2), can be solved by using the third-order strongly stable Runge-Kutta method [17], but the detailed formula is omitted for simplicity.

2.2. Canonical WENO schemes

The fifth-order WENO-JS scheme [4] is very popular ever since it was invented, and higher-order schemes [16] are developed based on the JS weights. For the fifth-order WENO-JS scheme, of which $r = 3$, two-degree polynomial approximation of the numerical flux function can be given as

$$\hat{f}_k(x) = a_{0,k} + a_{1,k}x + a_{2,k}x^2, \quad k = 0,1,2. \tag{8}$$

Specifically, the numerical flux functions of the candidate stencils for the approximation at grid half point $i+\frac{1}{2}$ are

$$\begin{aligned}
\hat{f}_{0,i+1/2} &= \frac{1}{6}(2f_{i-2} - 7f_{i-1} + 11f_i), \\
\hat{f}_{1,i+1/2} &= \frac{1}{6}(-f_{i-1} + 5f_i + 2f_{i+1}), \\
\hat{f}_{2,i+1/2} &= \frac{1}{6}(2f_i + 5f_{i+1} - f_{i+2}).
\end{aligned} \tag{9}$$

The error of the approximation in Eq.(9) can be obtained by Taylor expansion analysis, i.e.

$$\hat{f}_{k,i+1/2} = h_{k,i+1/2} + C_k\Delta x^3 + O(\Delta x^4), \tag{10}$$

where C_k is a constant which is independent of Δx but related to specific candidate stencils.

The weight of each numerical flux function of a candidate stencil, i.e. Eq.(6), is defined as

$$\omega_k = \frac{\alpha_k}{\sum_{k=0}^{r-1}\alpha_k}, \quad \alpha_k = \frac{d_k}{(\beta_k + \varepsilon)^q}. \tag{11}$$

The optimal linear weights d_k of fifth-order WENO schemes are

$$d_0 = 0.1, \quad d_1 = 0.6, \quad d_2 = 0.3, \tag{12}$$

which will generate the fifth-order background linear scheme on a five-point full stencil, and $\varepsilon = 10^{-6}$ is the small value avoiding zero denominator. It should be noticed that the small value also acts as a cutoff of the smoothness measurement [18], and has been modified to avoid overwhelming small measurements [6]. The exponent is usually defined as $q = 2$.

The nonlinear weights in Eq.(11) is essential to suppress the oscillations crossing discontinuities, ensuring the essentially non-oscillatory property. In general, the nonlinear weights corresponding to oscillatory stencils will be decreased, approximately removing the contribution of those stencils. Therefore, it is crucial to measure the smoothness of the flow field. The local smoothness indicator $\beta_{k,r}$ in the nonlinear weights determines the smoothness of each stencil to the final high order reconstruction, and is defined following Jiang and Shu [4], as

$$\beta_{k,r} = \sum_{j=1}^{r-1}\Delta x^{2j-1}\int_{x_{i-1/2}}^{x_{i+1/2}}\left(\frac{d^j}{dx^j}\hat{f}(x)\right)^2 dx. \tag{13}$$

Jiang and Shu [4] gave the explicit form of the local smoothness indicator $\beta_{k,r=3}$ of fifth-order schemes in terms of the numerical flux function f_i, i.e.

$$\begin{aligned}
\beta_0 &= \frac{1}{4}(f_{i-2} - 4f_{i-1} + 3f_i)^2 + \frac{13}{12}(f_{i-2} - 2f_{i-1} + f_i)^2, \\
\beta_1 &= \frac{1}{4}(f_{i-1} - f_{i+1})^2 + \frac{13}{12}(f_{i-1} - 2f_i + f_{i+1})^2, \\
\beta_2 &= \frac{1}{4}(3f_i - 4f_{i+1} + f_{i+2})^2 + \frac{13}{12}(f_i - 2f_{i+1} + f_{i+2})^2,
\end{aligned} \tag{14}$$

where the subscript r is omitted for simplicity.

2.3. TENO schemes

Two features of TENO schemes are more essential for introducing the method in this article. Firstly, the stencils of incrementally increasing width, with which arbitrary high-order spatial accuracy are achieved under TENO framework, are introduced. Secondly, the ENO-like stencil-selection procedure that ensures recovering the background linear schemes is a necessity needed to be introduced.

2.3.1. Incremental-width stencils

The candidate stencils of the fifth-order TENO scheme are the same as those of WENO schemes. However, incrementally increasing width stencils are used in higher-order TENO schemes. For attaining seventh-order spatial accuracy on a seven-point full stencil, TENO schemes use two four-point stencils, in addition to the three three-point stencils of the fifth-order TENO scheme. The stencils are schematically shown in Fig.1(b). The seventh-order WENO schemes use four four-point stencils, as shown in Fig.1(a), and in a very high order WENO scheme, the large sub-stencils enhance encounters of interacting characteristics, requiring specific treatment to avoid nonexistence of a smooth stencil [19]. On the other hand, TENO schemes are more suitable to deal with closely located shock waves such as those in compressible turbulence problem.

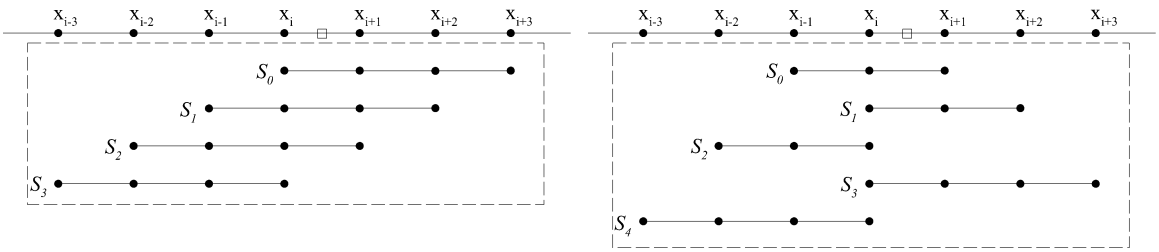

(a) The candidate stencils of seventh-order WENO schemes

(b) The candidate stencils of the seventh-order TENO scheme

Fig 1. Schematics illustrating the candidate stencils of seventh-order WENO and TENO schemes.

The details of seventh-order or even higher order TENO schemes, including the construction of candidate stencils and the optimal linear weights of those stencils, were introduced in [1] and are not further discussed here.

2.3.2. ENO-like stencil-selection procedure

The ENO-like stencil-selection procedure helps TENO schemes separating the shock/discontinuity-detection and high-order spatial reconstruction, allowing significant flexibility.

Motivated by Borges et al. [6] and Hu et al. [20] , the smoothness measurement of TENO schemes with

K-point full stencil is given as

$$\gamma_k = \left(C + \frac{\tau_K}{\beta_{k,r} + \varepsilon} \right)^q, \quad k = 0, \cdots, K-3. \tag{15}$$

The local smoothness indicator $\beta_{k,r}$ is the same as those in WENO schemes. The global reference smoothness indicator τ_K was detailed in [1], and for the fifth-order TENO scheme τ_5 is reused from WENO-Z scheme. The small threshold is defined as $\varepsilon = 10^{-40}$. C is set as 1, and the integer power q is set as 6. As introduced by Fu et al. [1], larger integer power exponent q and smaller C are preferable for a stronger separation between resolved and non-resolved scales, and the discontinuity-detection capability can be significantly enhanced.

TENO schemes do not directly use Eq.(15) to give the final weights. Instead, the smoothness measurement in Eq.(15) is normalised at first, i.e.

$$\chi_k = \frac{\gamma_k}{\sum_{k=0}^{K-3} \gamma_k}, \tag{16}$$

and then a cut-off procedure is defined as

$$\delta_k = \begin{cases} 0, & \text{if} \quad \chi_k < C_T, \\ 1, & \text{otherwise.} \end{cases} \tag{17}$$

Finally, the weights of TENO scheme are defined by a normalizing procedure

$$\omega_k^{(T)} = \frac{d_k \delta_k}{\sum_{k=0}^{K-3} d_k \delta_k}, \tag{18}$$

where the optimal weights are utilised without rescaling, and only the stencil deemed to be containing discontinuity is removed from the final reconstruction completely. Therefore, the numerical robustness of TENO scheme can be ensured, and the optimal weight, d_k, as well as the accuracy and spectral properties is fully recovered in smooth regions.

3. Exploring TENO schemes as shock-detectors

As introduced in [15], TENO schemes can be acting as a shock-detection-stencil-selection procedure. In [15], six-point and eight-point TENO schemes are discussed, and the hierarchical voting strategy reduces the number of possible combinations in the stencil-selection process. In this section, the five-point TENO scheme is discussed following the idea in [15], to facilitate the introduction in the following sections.

A WENO scheme uses continuous nonlinear weight to calculate convex combinations. Therefore, there are infinite possible combinations since the weights are calculated by continuous function. Whereas, TENO schemes in fact only implement several combination of the candidate stencils, by the nonlinear ENO-like stencil selection procedure in Eq.(17). For the fifth-order TENO scheme, which has three stencils as shown in Fig.2, potential combinations include $\{S_0, S_1, S_2\}$, $\{S_0, S_1\}$, $\{S_1, S_2\}$, $\{S_0, S_2\}$, and $\{S_k\}$ if other two stencils are both crossing discontinuity, as shown in Fig.2(b). Especially, for each candidate stencil S_k, there are only two potential choices of the weight, i.e. $\{d_k, 0\}$, before the normalization procedure in Eq.(18).

Obviously, the numerical flux as Eq.(6) is constructed based on a combination of candidate stencils and can be represented as a single high-order polynomial, resulting the fifth-order upwind central scheme ($\{S_0, S_1, S_2\}$) or the four-point schemes ($\{S_0, S_1\}$ or $\{S_1, S_2\}$), etc. Numerically, using these single high-order polynomial reconstructions is equivalent to the original TENO scheme, discarding the weighting procedure completely. Therefore, the equivalent numerical fluxes of the fifth-order TENO scheme evaluated at $x_{i+1/2}$ are given as

$$\hat{f}^*_{m,i+1/2} = a_{m,i-2} f_{i-2} + a_{m,i-1} f_{i-1} + a_{m,i} f_i + a_{m,i+1} f_{i+1} + a_{m,i+2} f_{i+2}, \tag{19}$$

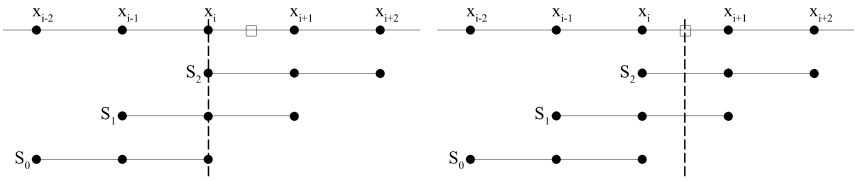

(a) A central stencil crossing discontinuity

(b) Two candidate stencils crossing discontinuity

Fig 2. Candidate stencils of a five-point (W/T)ENO scheme in the spatial approximation at $x_{i+\frac{1}{2}}$.

Table 1. The coefficients of the equivalent single polynomial spatial reconstructions.

if $\delta_{0,1,2} =$	$\hat{f}^*_{m,i+1/2}$	S^*_m	$a_{m,i-2}$	$a_{m,i-1}$	$a_{m,i}$	$a_{m,i+1}$	$a_{m,i+2}$
1,1,1	$\hat{f}^*_{0,i+1/2}$	S^*_0	1/30	-13/60	47/60	9/20	-1/20
0,1,1	$\hat{f}^*_{1,i+1/2}$	S^*_1	0	-1/9	2/3	1/2	-1/18
1,1,0	$\hat{f}^*_{2,i+1/2}$	S^*_2	1/21	-13/42	41/42	2/7	0
0,0,1	$\hat{f}^*_{3,i+1/2}$	S^*_3	0	0	1/3	5/6	-1/6
0,1,0	$\hat{f}^*_{4,i+1/2}$	S^*_4	0	-1/6	5/6	1/3	0
1,0,0	$\hat{f}^*_{5,i+1/2}$	S^*_5	1/3	-7/6	11/6	0	0
1,0,1	$\hat{f}^*_{6,i+1/2}$	S^*_6	1/12	-7/24	17/24	5/8	-1/8

where the subscript m is used for numbering the polynomials and distinguishing to the stencils using subscript k which relates to the local smoothness indicators. The coefficients of these polynomials are given in Table 1.

Here, $\hat{f}^*_{m,i+1/2}$ is constructed on S^*_m shown in Fig.3. Thereinto, $\hat{f}^*_{6,i+1/2}$ constructed on stencil S^*_6 is equivalent to the numerical flux constructed based on the combination of $\{S_0, S_2\}$, but it is not an actual continuous reconstruction or of fifth-order of accuracy.

It should be mentioned explicitly, only one numerical flux $\hat{f}^*_{m,i+1/2}$ needs to be be selected in the spatial reconstruction, equivalently representing a weighted averaged numerical flux of the original TENO scheme. This explanation brings flexibility to independently define the smoothness measurement and the spatial reconstructions, leading to more further possibilities.

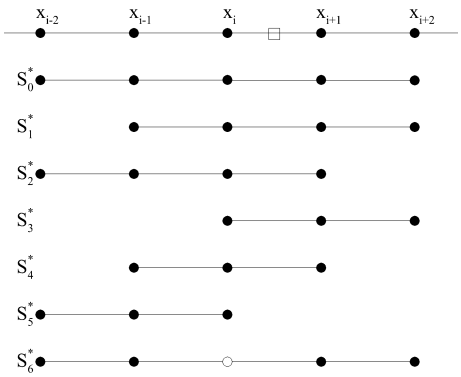

Fig 3. Schematic of the equivalent candidate stencils of the fifth-order TENO scheme. The circle indicates that the stencil is not really continuous.

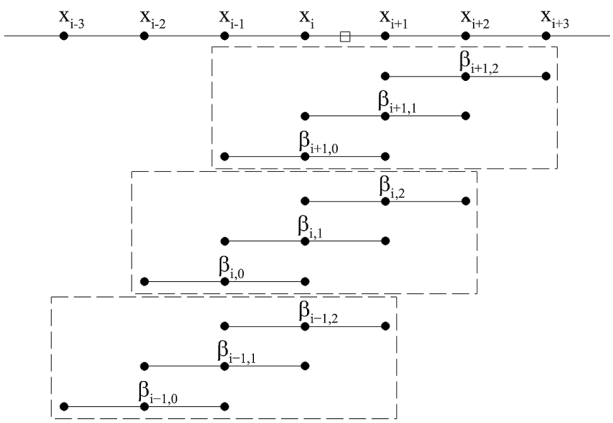

Fig 4. The neighbouring smoothness measurement to be explored.

4. The presented method

4.1. Exploiting neighbouring smoothness information

For TENO schemes, it is unnecessary to provide exact relative smoothness of each candidate stencil in constructing high-order polynomials. Examining the discontinuity-detection issue in the whole spatial field, it could be found that all the discontinuities can be effectively detected by using the smoothness measurement of the fifth-order TENO scheme [14]. In other word, the smoothness measurement works sufficiently well to provide the smoothness information of the whole field, as least in those typical gas dynamic problems. Therefore, if all the discontinuities are successfully detected, it might be possible to achieve arbitrary high-order interpolation as long as there is a sufficiently large smooth region.

However, the smoothness information can not be directly used in current frameworks. As shown in Fig.4, one may notices that in a five-point WENO or TENO scheme approximating the variables at $x_{i+1/2}$, only the information based on $\beta_{i,0}$, $\beta_{i,1}$ and $\beta_{i,2}$ can be applied to determine discontinuities or smooth field, and achieving fifth-order accuracy is the best result in this context, even the neighbouring five-point full stencils are all smooth.

It is obvious that the three five-point full stencils in Fig.4 cover the the same region as the seventh-order TENO scheme, and thus we can investigate this case. Examining the three five-point full stencils in Fig.4, one may find that they are overlapping with each other. Therefore, it is highly possible that one discontinuity is detected by more than one five-point full stencil. Examining the candidate stencils of the seventh-order TENO scheme, as shown in Fig.1(b), it is obvious that the candidate stencils of the fifth-order TENO scheme are included. As known, the leading term of the local smoothness indicator $\beta_{i,k}$ is of $\mathcal{O}(\Delta x^2)$ if the corresponding stencil is smooth. Otherwise, if a discontinuity is located in a certain stencil, the corresponding $\beta_{i,k}$ is of $\mathcal{O}(1)$, invoking the ENO-like stencil-selection procedure.

Therefore, in order to show the capability of the neighbouring smoothness measurement in providing effective information for constructing a higher-order approximation at $x_{i+1/2}$, following remarks are given.

Remark 1. Examining Figs.1(b) and 4, if a discontinuity is located within the range of the central five-point full stencil, one of the local smoothness indicators of the five-point full stencil or at least one of the local smoothness indicators of the seventh-point full stencil will be of $\mathcal{O}(1)$. If a discontinuity is located within the range of the seven-point full stencil, but outside the range of the central five-point full stencil, one of the local smoothness indicators of the neighbouring five-point full stencil or the seventh-point full stencil will be of $\mathcal{O}(1)$. Eventually, the discontinuity can be located accurately by using either the three five-point smoothness measurements in Fig.4 or the seven-point smoothness measurement in Fig.1(b). □

Remark 2. Regarding to attaining designed order of accuracy, the ENO-like selection procedure helps to give a relaxed condition [12] as

$$\frac{\tau_{i,5}}{\beta_{i,k}+\varepsilon} = O(\Delta x^s), \quad s > 0, \tag{20}$$

where $\tau_{i,5} = |\beta_{i,0} - \beta_{i,2}|$. This is the condition required for TENO schemes to restore the formal order of accuracy in smooth regions. In fact, as aforementioned, using Eq.(15) significantly enhances discontinuity-detection capability of the smoothness measurement, and the ENO-like stencil-selection procedure directly applies those optimal linear schemes, except for those oscillating stencils where discontinuities are located, i.e. where $\chi_k < C_t$. □

Remark 3. In hyperbolic system equations, e.g. Euler equations, characteristic-wise reconstruction is necessary to avoid oscillation [16]. Therefore, the matrix $\mathbf{L}$ which is the left eigenvectors of the Jacobian matrix $\mathbf{A} = \frac{\partial \mathbf{F}}{\partial \mathbf{U}}$ should be used to calculate the characteristic variables, i.e.

$$\mathbf{Q}_l = \mathbf{L}_{i+1/2} \cdot \mathbf{U}_l, \quad i-2 \le l \le i+2. \tag{21}$$

To be clear, here $\mathbf{F}$ and $\mathbf{U}$ are the numerical flux and the conservative variables of the hyperbolic system equations, respectively.

It is unnecessary to detail the characteristic-wise reconstruction procedure. However, it does need to notice that the three five-point smoothness measurements in Fig.4 are calculated based on the characteristic variables calculated using different Jacobian matrices, i.e. $\mathbf{A}_{i-1/2}$, $\mathbf{A}_{i+1/2}$ and $\mathbf{A}_{i+3/2}$. Luckily, in smooth field, the difference of linearised matrix $\mathbf{A}$, i.e. $\Delta\mathbf{A}$, is of $\mathscr{O}(\Delta x)$, and thus the characteristic variables calculated using $\mathbf{L}' = \mathbf{L} + \Delta\mathbf{L}$ does not change the essential property of the smoothness measurement. □

Eventually, for the one-dimensional field as shown in Fig.4, two neighbouring stencils are utilised in calculating the numerical flux at $x_{i+\frac{1}{2}}$. A binary vector storing the information of local smoothness is then given as

$$\Delta_i = (\delta_{i-1,0}, \delta_{i,0}, \delta_{i,1}, \delta_{i,2}, \delta_{i+1,2}). \tag{22}$$

4.2. Higher-order spatial reconstructions

In the last subsection, based on the smoothness measurement of the five-point TENO scheme, a method providing extra smoothness information is given, and thus higher-order polynomials can be used in the smooth region. In [15], predefined optimal linear schemes are implemented as candidate spatial reconstructions. A similar idea is given as follows.

Here, up to seventh-order candidate reconstructions are given, directly using two extra neighbouring points of five-point schemes. Similar to Eq.(19), all the numerical fluxes evaluated at $x_{i+1/2}$ are given as an unified form,

$$\hat{f}^{**}_{m,i+1/2} = \sum_{l=i-3}^{i+3} a_{m,l} f_l, \tag{23}$$

and the coefficients are given in Table 2.

Examining these coefficients, compared with the stencils in Fig.3, we can simply find that apart from the original high-order representatives, the presented method exploits several higher-order polynomials, including the seventh-order polynomial $\hat{f}^{**}_{0,i+1/2}$, sixth-order polynomials $\hat{f}^{**}_{1,i+1/2}$ and $\hat{f}^{**}_{2,i+1/2}$, and also two more fifth-order polynomials, i.e. $\hat{f}^{**}_{3,i+1/2}$ and $\hat{f}^{**}_{5,i+1/2}$, as well as two forth-order polynomials $\hat{f}^{**}_{6,i+1/2}$ and $\hat{f}^{**}_{9,i+1/2}$. All these newly introduced high-order reconstructions are constructed with using the two extra neighbouring points. At the mean time, the coefficients of $\hat{f}^{**}_{7,i+1/2}$ and $\hat{f}^{**}_{8,i+1/2}$ are different to those forth-order polynomials in Table 1, even they are using the same stencils. This is because the coefficients in Table 1 are calculated using the optimal linear weights in Eq.(12), after the ENO-like selection. Moreover, the stencil, S^*_6, is discarded since it is in fact crossing a central discontinuity.

Table 2. The coefficients of the numerical flux functions of the presented method.

$\hat{f}^{**}_{m,i+1/2}$	$a_{m,i-3}$	$a_{m,i-2}$	$a_{m,i-1}$	$a_{m,i}$	$a_{m,i+1}$	$a_{m,i+2}$	$a_{m,i+3}$
$\hat{f}^{**}_{0,i+1/2}$	-1/140	5/84	-101/420	319/420	107/210	-19/210	1/105
$\hat{f}^{**}_{1,i+1/2}$	0	1/60	-2/15	37/60	37/60	-2/15	1/60
$\hat{f}^{**}_{2,i+1/2}$	-1/60	7/60	-23/60	19/20	11/30	-1/30	0
$\hat{f}^{**}_{3,i+1/2}$	0	0	-1/20	9/20	47/60	-13/60	1/30
$\hat{f}^{**}_{4,i+1/2}$	0	1/30	-13/60	47/60	9/20	-1/20	0
$\hat{f}^{**}_{5,i+1/2}$	-1/20	17/60	-43/60	77/60	1/5	0	0
$\hat{f}^{**}_{6,i+1/2}$	0	0	0	1/4	13/12	-5/12	1/12
$\hat{f}^{**}_{7,i+1/2}$	0	0	-1/12	7/12	7/12	-1/12	0
$\hat{f}^{**}_{8,i+1/2}$	0	1/12	-5/12	13/12	1/4	0	0
$\hat{f}^{**}_{9,i+1/2}$	-1/4	13/12	-23/12	25/12	0	0	0
$\hat{f}^{**}_{10,i+1/2}$	0	0	0	1/3	5/6	-1/6	0
$\hat{f}^{**}_{11,i+1/2}$	0	0	-1/6	5/6	1/3	0	0
$\hat{f}^{**}_{12,i+1/2}$	0	1/3	-7/6	11/6	0	0	0

Table 3. The coefficients of the numerical flux functions of the presented method. (* indicates 1 or 0)

$\Delta_i =$	$\hat{f}^{**}_{m,i+1/2}$	$\Delta_i =$	$\hat{f}^{**}_{m,i+1/2}$
$(1,1,1,1,1)$	$\hat{f}^{**}_{0,i+1/2}$	$(*,0,1,1,0)$	$\hat{f}^{**}_{7,i+1/2}$
$(0,1,1,1,1)$	$\hat{f}^{**}_{1,i+1/2}$	$(0,1,1,0,*)$	$\hat{f}^{**}_{8,i+1/2}$
$(1,1,1,1,0)$	$\hat{f}^{**}_{2,i+1/2}$	$(1,1,0,0,*)$	$\hat{f}^{**}_{9,i+1/2}$
$(*,0,1,1,1)$	$\hat{f}^{**}_{3,i+1/2}$	$(*,*,0,1,0)$	$\hat{f}^{**}_{10,i+1/2}$
$(0,1,1,1,0)$	$\hat{f}^{**}_{4,i+1/2}$	$(*,0,1,0,*)$	$\hat{f}^{**}_{11,i+1/2}$
$(1,1,1,0,*)$	$\hat{f}^{**}_{5,i+1/2}$	$(0,1,0,0,*)$	$\hat{f}^{**}_{12,i+1/2}$
$(*,*,0,1,1)$	$\hat{f}^{**}_{6,i+1/2}$	$(*,0,0,0,*)$	no exist

Eventually, we can find the basic features of the presented method. Firstly, all the final reconstructions do not cross any discontinuity. In fact, WENO schemes or the TENO schemes before [15] are possible to calculate the final approximation using the numerical fluxes in both sides of a discontinuity. For example, in Fig.2(a), the central stencil could be discarded but the other two stencils could be applied. Secondly, the presented method is also suitable to deal with multiple closely located shocklets, because the polynomial constructed on a smaller stencil could be applied in such case.

4.3. The stencil-selection procedure

The TENO framework allows the separation of high-order spatial reconstructions and smoothness measurement. For calculating the high-order polynomials introduced in the last subsection, the smoothness information should be provided at first, which means that the local smoothness indicators, $\beta_{i,k}$, as well as the global smoothness indicators $\tau_{i,5}$, should be readily available before the spatial reconstructions, providing the binary vector in Eq.(22). In this work, the method calculating the local and global smoothness indicators is the same as that of the fifth-order TENO scheme, and thus the binary vector storing smoothness information can be calculated trivially. The relation between this binary vector and the implementation of the high-order reconstructions in Table 2 is then given in Table 3.

It should be noticed that there are 2^5=32 possible combinations of Eq.(22), and each of them is correspondent to a numerical flux reconstruction, except that the three central smoothness indicators can not be all oscillatory and reconstructions crossing discontinuity are completely avoided. Moreover, two situations need to be further explained. First, if $\Delta_i = (1,1,0,1,1)$, this is, theoretically, available for using $\hat{f}^{**}_{6,i+1/2}$ and $\hat{f}^{**}_{9,i+1/2}$. However, considering that the numerical flux at $x_{i+1/2}$ is to be evaluated, $\hat{f}^{**}_{6,i+1/2}$ is used to make this evaluation an interpolation, instead of an extrapolation while using $\hat{f}^{**}_{9,i+1/2}$. Second, similar to the first case, $\Delta_i = (1,1,0,1,0)$ is correspondent to $\hat{f}^{**}_{10,i+1/2}$, instead of $\hat{f}^{**}_{9,i+1/2}$.

By exploring the ENO-like selection procedure, a wider stencil can be used without amending the original five-point smoothness measurement. As mentioned in the beginning of this subsection, the smoothness measurement of the whole computation domain should be calculated before the spatial reconstruction, for

providing the neighbouring smoothness information, and the smoothness information should be stored in the calculation of $\hat{f}_{i\pm1/2}$.

4.4. A further improvement for solving scalar equations

In order to further improve the efficiency of solving scalar equations, which does not require the complex calculation of characteristic-wise variables, we redefine the local smooth indicators as

$$\beta_i = \frac{1}{4}(f_{i-1} - f_{i+1})^2 + \frac{13}{12}(f_{i-1} - 2f_i + f_{i+1})^2, \tag{24}$$

and

$$\begin{aligned} \beta_0 &= \beta_{i-1}, \\ \beta_1 &= \beta_i, \\ \beta_2 &= \beta_{i+1}. \end{aligned} \tag{25}$$

Then the following procedure can follow that of TENO schemes. Comparing with the smoothness measurement in Fig.4, the computational cost will significantly reduced. The simplified scheme is then denoted as TENO5-SE.

5. Numerical results

5.1. Approximate dispersion relation analysis

Approximate dispersion relation (ADR) analysis [22] is performed at first. As shown in Fig.5, TENO schemes and the presented methods show agreement with the background linear schemes in low and intermediate wave number. In high wave number region, the results of the nonlinear schemes deviate from the results of the background linear schemes. Especially, the TENO-E methods which use the smoothness measurement of the fifth-order TENO scheme, deviates from the seventh-order linear scheme at the same wave number which causes deviation between the fifth-order TENO scheme and its background linear scheme.

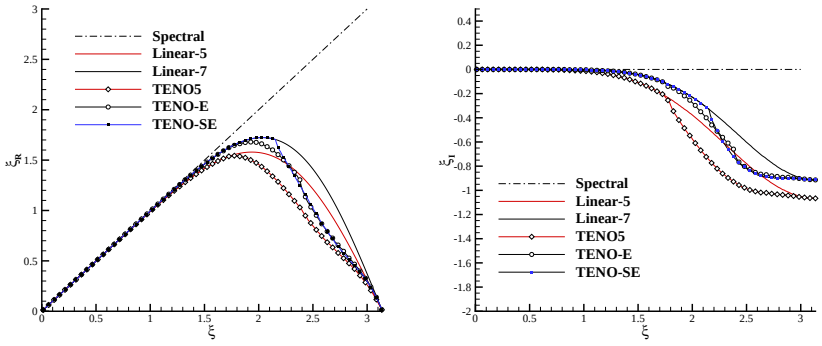

(a) dispersion (b) dissipation

Fig 5. The approximate dispersion and the dissipation properties of the presented method.

5.2. One-dimensional linear advection problem

A scalar linear advection problem having a smooth field is then applied in this section. The equation to be solved is

$$\frac{\partial u}{\partial t} + \frac{\partial u}{\partial x} = 0, \tag{26}$$

and the initial condition is

$$u_0(x) = e^{-300(x-x_c)^2}, \quad x_c = 0.5. \tag{27}$$

Periodic boundary condition is used to model the infinite one-dimensional scalar field. The solution at $t = 1$ and between $x = 0$ and $x = 1$, which is one period of the solution, is investigated with using uniformly refined spatial discretization, and the time steps are sufficiently refined to achieve the convergence of temporal solutions.

In Fig.6, the L_1 and L_∞ error of several schemes are presented. It is shown that except for coarse discretizations, the resolution and accuracy of TENO schemes and the presented methods are the same as those of the linear schemes. Whereas, WENO-JS5 scheme is showing lower resolution, although its convergence is also approximately fifth-order. WENO-JS7 scheme [16] does not achieve seventh-order accuracy in this case. In general, it can be concluded that the presented schemes have indeed recovered the background linear scheme in the smooth field.

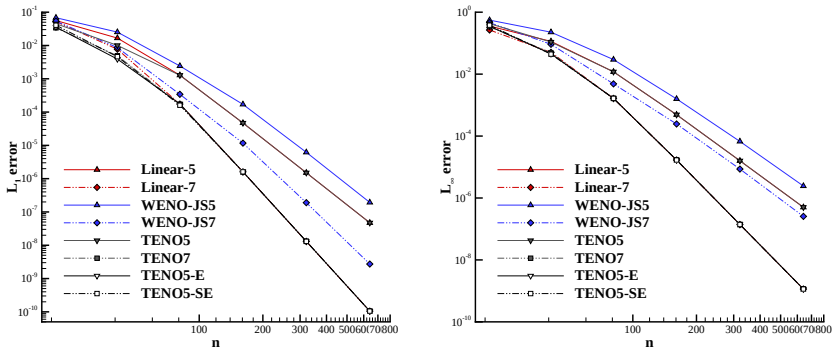

(a) L_1 error (b) L_∞ error

Fig 6. The convergence of the simulation of the 1D scalar linear advection problem.

5.3. Shock wave-density wave interaction problem

In order to investigate the performance in resolving smooth critical points, a classical one-dimensional test case in [24] is applied. In this case, a Mach 3 shockwave travels along the shock-tube, interacting with sine wave in density. TENO scheme has shown superiority in this case [1]. Here, seven-point TENO schemes and the presented method (TENO5-E) are used for comparison.

The computation domain is $[-5, 5]$, and discretized by 200 equidistant distributed grid points. The initial condition is designed as

$$(\rho, u, p) = \begin{cases} (3.8571, 2.6294, 10.3333), & \text{if} \quad x \leq -4, \\ (1 + 0.2\sin(5x), 0, 1), & \text{if} \quad x > -4, \end{cases} \tag{28}$$

Fig.7(a) shows the density distributions at $t = 1.8$ of the numerical results. The result of the five-point WENO-JS scheme with using 2000 grid points is used as the reference result, since there is not a theoretically exact solution.

It can be found that the presented method shows similar result in resolving smooth wave structure, comparing with the TENO-7 scheme. We have also compared the results of WENO-JS-(5/7) and TENO-5 schemes, and the advantage of the presented method will be more significant. Those results are not shown for simplicity.

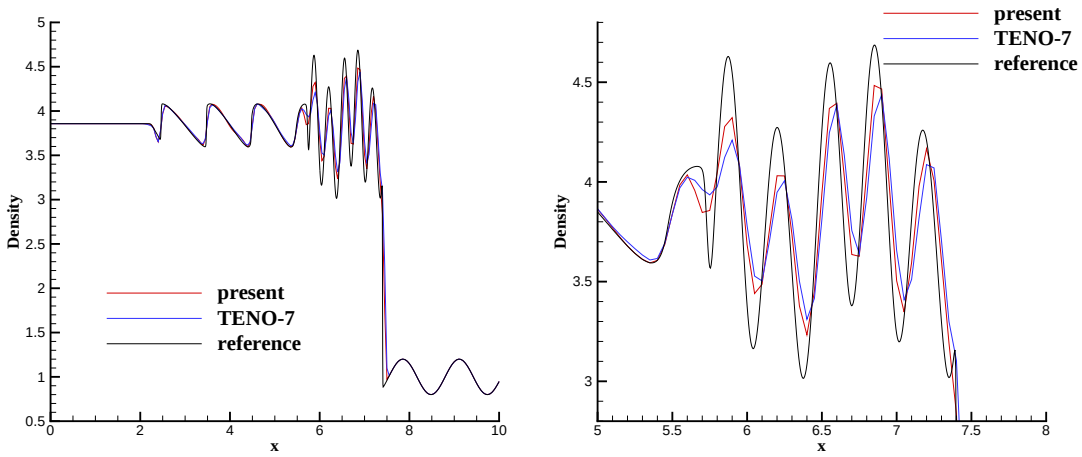

Fig 7. The density distribution of shock-density wave interaction problem.

6. Conclusions

In this paper, simple extending strategies based on the smoothness measurement of the fifth-order TENO scheme is introduced. Up to seventh-order accuracy is achieved without significant extra computation effort.

References

[1] Lin Fu, Xiangyu Y. Hu, and Nikolaus A. Adams. A family of high-order targeted eno schemes for compressible-fluid simulations. Journal of Computational Physics, 305:333–359, 2016.

[2] Xu Dong Liu, Stanley Osher, and Tony Chan. Weighted essentially non-oscillatory schemes. Journal of Computational Physics, 115(1):200–212, November 1994.

[3] Ami Harten, Bjorn Engquist, Stanley Osher, and Sukumar R Chakravarthy. Uniformly high order accurate essentially non-oscillatory schemes, III. Journal of Computational Physics, 71(2):231–303, August 1987.

[4] Guang-Shan Jiang and Chi-Wang Shu. Efficient implementation of weighted ENO schemes. Journal of Computational Physics, 126(1):202–228, June 1996.

[5] Andrew K. Henrick, Tariq D. Aslam, and Joseph M. Powers. Mapped weighted essentially non-oscillatory schemes: Achieving optimal order near critical points. Journal of Computational Physics, 207(2):542–567, 2005.

[6] Rafael Borges, Monique Carmona, Bruno Costa, and Wai Sun Don. An improved weighted essentially non-oscillatory scheme for hyperbolic conservation laws. Journal of Computational Physics, 227(6):3191–3211, 2008.

[7] I.W. Kokkinakis and D. Drikakis. Implicit large eddy simulation of weakly-compressible turbulent channel flow. Computer Methods in Applied Mechanics and Engineering, 287:229 – 261, 2015.

[8] Konstantinos Ritos, Ioannis W. Kokkinakis, and Dimitris Drikakis. Physical insight into the accuracy of finely-resolved iles in turbulent boundary layers. Computers & Fluids, 169:309 – 316, 2018.

[9] Konstantinos Ritos, Ioannis W. Kokkinakis, and Dimitris Drikakis. Performance of high-order implicit large eddy simulations. Computers & Fluids, 2018.

[10] Xin-Liang Li, De-Xun Fu, Yan-Wen Ma, and Xian Liang. Direct numerical simulation of compressible turbulent flows. Acta Mechanica Sinica, 26(6):795–806, Dec 2010.

[11] Fulin Tong, Xinliang Li, Yanhui Duan, and Changping Yu. Direct numerical simulation of supersonic turbulent boundary layer subjected to a curved compression ramp. Physics of Fluids, 29(12):125101, 2017.

[12] Lin Fu, Xiangyu Y. Hu, and Nikolaus A. Adams. Targeted ENO schemes with tailored resolution property for hyperbolic conservation laws. Journal of Computational Physics, 349:97–121, 2017.

[13] Ory Haimovich and Steven H. Frankel. Numerical simulations of compressible multicomponent and multiphase flow using a high-order targeted ENO (TENO) finite-volume method. Computers & Fluids, 146:105–116, 2017.

[14] Haibo Dong, Lin Fu, Fan Zhang, Yu Liu, and Jun LIU. Detonation simulations with a fifth-order teno scheme. Communications in Computational Physics, 2018.

[15] Lin Fu, Xiangyu Y. Hu, and Nikolaus A. Adams. A new class of adaptive high-order targeted eno schemes for hyperbolic conservation laws. Journal of Computational Physics, 2018.

[16] Dinshaw S. Balsara and Chi-Wang Shu. Monotonicity preserving weighted essentially non-oscillatory schemes with increasingly high order of accuracy. Journal of Computational Physics, 160(2):405 – 452, 2000.

[17] S. Gottlieb, C. Shu, and E. Tadmor. Strong stability-preserving high-order time discretization methods. SIAM Review, 43(1):89–112, 2001.

[18] Marcos Castro, Bruno Costa, and Wai Sun Don. High order weighted essentially non-oscillatory weno-z schemes for hyperbolic conservation laws. Journal of Computational Physics, 230(5):1766–1792, 2011.

[19] G.A. Gerolymos, D. Sénéchal, and I. Vallet. Very-high-order WENO schemes. Journal of Computational Physics, 228(23):8481 – 8524, 2009.

[20] X.Y. Hu and N.A. Adams. Scale separation for implicit large eddy simulation. Journal of Computational Physics, 230(19):7240–7249, 2011.

[21] Lin Fu. A low-dissipation finite-volume method based on a new teno shock-capturing scheme. Computer Physics Communications, 2018.

[22] Sergio Pirozzoli. On the spectral properties of shock-capturing schemes. Journal of Computational Physics, 219(2):489 – 497, 2006.

[23] Meiliang Mao, Zhenguo Yan, Huayong Liu, Huajun Zhu, and Xiaogang Deng. Study of quasi-linear spectral analysis method of high-order weighted nonlinear schemes. Acta Aerodynamica Sinica, 33(1):1–9, 2015.

[24] Chi-Wang Shu and Stanley Osher. Efficient implementation of essentially non-oscillatory shock-capturing schemes,ii. J. Comput. Phys., 83(1):32–78, July 1989.